

## Short Communication

Enhanced production of benzyl alcohol in the gas phase continuous hydrogenation of benzaldehyde over Au/Al<sub>2</sub>O<sub>3</sub>

Maoshuai Li, Xiaodong Wang, Noémie Perret, Mark A. Keane\*

Chemical Engineering, School of Engineering and Physical Sciences, Heriot-Watt University, Edinburgh EH14 4AS, Scotland, United Kingdom

## ARTICLE INFO

## Article history:

Received 28 October 2013

Received in revised form 12 December 2013

Accepted 18 December 2013

Available online 24 December 2013

## Keywords:

Benzaldehyde

Selective hydrogenation

Benzyl alcohol

Au/Al<sub>2</sub>O<sub>3</sub>

Water as carrier

## ABSTRACT

Exclusive hydrogenation of benzaldehyde to benzyl alcohol in gas phase continuous operation (393–413 K, 1 atm) was achieved over Au/Al<sub>2</sub>O<sub>3</sub>, Au/TiO<sub>2</sub> and Au/ZrO<sub>2</sub>. Synthesis of Au/Al<sub>2</sub>O<sub>3</sub> by deposition–precipitation generated a narrower distribution (2–8 nm) of smaller (mean = 4.3 nm) Au particles relative to impregnation (1–21 nm, mean = 7.9 nm) with increased H<sub>2</sub> uptake under reaction conditions and higher benzaldehyde turnover. Switching reactant carrier from ethanol to water resulted in a significant enhancement of selective hydrogenation rate over Au/Al<sub>2</sub>O<sub>3</sub> with 100% benzyl alcohol yield, attributed to increased available reactive hydrogen. This response extends to reaction over Au/TiO<sub>2</sub> and Au/ZrO<sub>2</sub>.

© 2013 Elsevier B.V. All rights reserved.

## 1. Introduction

Benzyl alcohol is widely utilised as a solvent for inks, paints and lacquers and as precursor to a range of esters in the cosmetics and flavouring industries [1]. Industrial production via benzyl chloride hydrolysis releases chlorine with significant by-product (benzyl ether and NaCl) formation while toluene oxidation consumes large quantities of solvents with the inclusion of toxic bromides to enhance alcohol yield [2,3]. As an alternative, benzaldehyde hydrogenation has been promoted over Rh and Ru complexes using alcohols and organic acids as hydrogen donors [4,5]. Product separation and catalyst reuse are facilitated by switching to heterogeneous systems. Application of solid catalysts has focused on liquid phase reaction over Ni, Ru, Pt and Pd on a range of supports (monolith, Al<sub>2</sub>O<sub>3</sub>, activated carbon and SiO<sub>2</sub>) [6–9]; pertinent conversion/selectivity and associated reaction conditions are compiled in Table 1. Okamoto and co-workers [9] recorded 100% alcohol selectivity at partial aldehyde conversion (84%) over polyethylene glycol (PEG) modified Pd/SiO<sub>2</sub>. Zhao et al. [10] achieved near complete benzaldehyde conversion and full selectivity to benzyl alcohol over Pt/C at elevated H<sub>2</sub> pressure (4 MPa). Gas phase continuous operation has employed a series of metal oxides (ZnO, Fe<sub>2</sub>O<sub>3</sub>, Al<sub>2</sub>O<sub>3</sub>, ZrO<sub>2</sub>, CeO<sub>2</sub> and TiO<sub>2</sub>) [11] and oxide supported Pt, Cu and Ni [12–14]. Supported Pt exhibited superior performance with full selectivity to the alcohol at conversions up to 80% over Pt/TiO<sub>2</sub> (Table 1), attributed to C=O activation at the metal-support interface [12]. Product distribution over supported Cu was dependent on support and temperature where Cu/SiO<sub>2</sub> delivered high selectivity (83% at 373 K) but there was

no detectable alcohol formation over Cu on Al<sub>2</sub>O<sub>3</sub>, TiO<sub>2</sub>, CeO<sub>2</sub> or ZrO<sub>2</sub> irrespective of temperature [13]. Exclusive C=O reduction, circumventing hydrogenolysis and phenyl ring reduction at high conversions remains challenging [14].

Oxide supported Au has exhibited enhanced chemoselectivity in the hydrogenation of aldehydes and ketones relative to standard transition metal catalysts [15,16]. This is offset somewhat by lower reaction rates due to the lesser capacity of Au for H<sub>2</sub> activation [16]. In previous work, we reported exclusive hydrogenation of benzaldehyde to benzyl alcohol over Au/Al<sub>2</sub>O<sub>3</sub> (prepared by impregnation) under conditions where Ni/Al<sub>2</sub>O<sub>3</sub> and Pd/Al<sub>2</sub>O<sub>3</sub> were non-selective [17]. Complete selectivity over Au/Al<sub>2</sub>O<sub>3</sub> was obtained at low hydrogenation rates (conversion ≤ 15%). As an extension to that work, we have evaluated the catalytic action of Au/Al<sub>2</sub>O<sub>3</sub> prepared by deposition–precipitation to generate smaller Au size. Moreover, we demonstrate for the first time the use of water as an environmentally benign aldehyde carrier to elevate catalytic productivity in continuous gas phase operation (at 0.1 MPa) with 100% alcohol yield. We also assess the catalytic performance of Au/TiO<sub>2</sub> and Au/ZrO<sub>2</sub> to validate the promotional effect of water.

## 2. Experimental

## 2.1. Catalyst preparation and activation

The γ-Al<sub>2</sub>O<sub>3</sub> (Puralox, Condea Vista) and TiO<sub>2</sub> (P25, Degussa) supports were used as received. The ZrO<sub>2</sub> carrier was synthesised by ZrOCl<sub>2</sub> (0.1 M) precipitation with aqueous NH<sub>3</sub> (2.5 M) under vigorous stirring (600 rpm) at pH 9.4–11.8. The hydrogel was dried at 373 K (24 h) and calcined (1 K min<sup>-1</sup>) in 60 cm<sup>3</sup> min<sup>-1</sup> air at 673 K (5 h).

\* Corresponding author. Tel.: +44 131 451 4719.

E-mail address: [M.A.Keane@hw.ac.uk](mailto:M.A.Keane@hw.ac.uk) (M.A. Keane).

**Table 1**

Conversions (*X*) and selectivities (*S*) with associated temperatures and pressures reported for benzaldehyde hydrogenation.

Catalyst	Phase	<i>T</i> (K)	<i>P</i> <sub>H<sub>2</sub></sub> (MPa)	<i>X</i> (%)	<i>S</i> (%)	Ref.
PEG-Pd/SiO <sub>2</sub>	Liquid	453	3	84	100	[9]
Pt/C	Liquid	323	4	98	100	[10]
Pt/TiO <sub>2</sub>	Gas	453	0.1	80	100	[12]
Cu/SiO <sub>2</sub>	Gas	373	0.1	68	83	[13]
Au/Al <sub>2</sub> O <sub>3</sub>	Gas	393	0.1	15	100	[17]

Alumina supported Au prepared by impregnation (Au/Al<sub>2</sub>O<sub>3</sub>-IMP) is described in detail elsewhere [17]. Synthesis by deposition–precipitation (Au/Al<sub>2</sub>O<sub>3</sub>-DP, Au/ZrO<sub>2</sub> and Au/TiO<sub>2</sub>) employed an aqueous solution of urea (100 fold excess) and HAuCl<sub>4</sub> ( $5 \times 10^{-4}$  M) with support addition, heating the suspension to 353 K (2 K min<sup>-1</sup>), which was maintained for 3 h with a pH increase to ca. 7. The solid was washed and dried in He (45 cm<sup>3</sup> min<sup>-1</sup>) at 373 K (2 K min<sup>-1</sup>) for 5 h. Catalyst precursors were sieved into a batch of 75 μm average diameter and activated at 2 K min<sup>-1</sup> to 473–603 K in 60 cm<sup>3</sup> min<sup>-1</sup> H<sub>2</sub>.

## 2.2. Catalyst characterisation

Gold content was determined by atomic absorption spectroscopy (Shimadzu AA-6650 spectrometer). Temperature programmed reduction (TPR) and H<sub>2</sub> chemisorption were recorded on the commercial CHEM-BET 3000 (Quantachrome) unit, as described previously [17]. Nitrogen adsorption–desorption isotherms were obtained using the Micromeritics Gemini 2390 system where total surface area was determined using the standard BET method and cumulative pore volumes by BJH analysis. Powder X-ray diffractograms (XRD) were recorded on a Bruker/Siemens D500 incident X-ray diffractometer. Diffractograms were identified using JCPDS-ICDD reference standards, i.e. Au (Card No. 04-0784) and γ-Al<sub>2</sub>O<sub>3</sub> (10-0425). Gold particle size and morphology were determined by transmission (TEM, JEOL JEM 2011) and scanning transmission (STEM, JEOL 2200FS) electron microscopy. Samples for analysis were prepared by dispersion in acetone and deposited on a holey carbon/Cu grid (300 Mesh). Surface area weighted mean Au size (*d*<sub>TEM</sub>) was obtained from a count of at least 300 particles.

## 2.3. Catalytic procedure

Catalyst testing was carried out in situ after activation in a continuous flow fixed-bed tubular reactor (*i.d.* = 15 mm, *l* = 30 cm). Isothermal conditions (393–423 ± 1 K) were maintained by diluting the catalyst with ground glass (75 μm). Benzaldehyde was delivered as ethanolic or aqueous solutions via a glass/teflon air-tight syringe and teflon line using a microprocessor controlled infusion pump (Model 100 kd Scientific). A co-current flow of benzaldehyde and H<sub>2</sub> was maintained at GHSV = 2 × 10<sup>4</sup> h<sup>-1</sup> with an inlet benzaldehyde flow (*F*) of

**Table 2**

Physico-chemical characteristics of the supported Au catalysts.

Catalyst	Au/Al <sub>2</sub> O <sub>3</sub> -DP	Au/Al <sub>2</sub> O <sub>3</sub> -IMP	Au/TiO <sub>2</sub>	Au/ZrO <sub>2</sub>
Au loading (%w/w)	1.1	1.1	1.2	0.8
BET area (m <sup>2</sup> g <sup>-1</sup> )	166	161	48	93
Pore volume (cm <sup>3</sup> g <sup>-1</sup> )	0.36	0.36	0.12	0.13
TPR <i>T</i> <sub>max</sub> (K)	450	415	364	452
Measured TPR H <sub>2</sub> consumption (μmol g <sup>-1</sup> )	87	79	126	56
Theoretical <sup>a</sup> TPR H <sub>2</sub> consumption (μmol g <sup>-1</sup> )	84	80	91	61
H <sub>2</sub> chemisorption (μmol g <sub>Au</sub> <sup>-1</sup> ) at 413 K	318	45	162	137
Au particle size range (nm)	2–8	1–21	2–9	3–12
<i>d</i> <sub>TEM</sub> (nm)	4.3	7.9	4.5	7.0

<sup>a</sup> Amount required for Au precursor reduction.

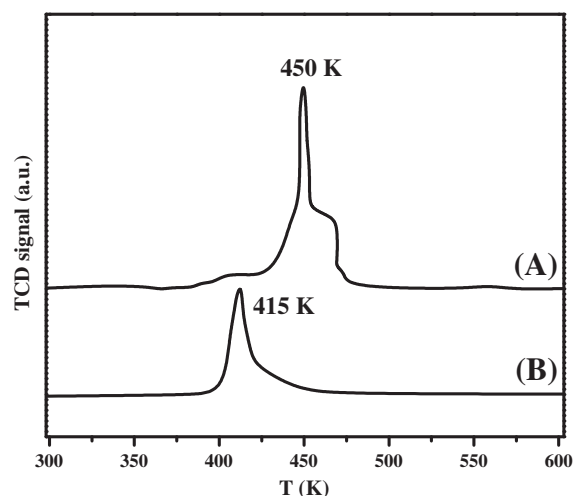


Fig. 1. TPR profiles for (A) Au/Al<sub>2</sub>O<sub>3</sub>-DP and (B) Au/Al<sub>2</sub>O<sub>3</sub>-IMP.

$4.8 \times 10^{-5}$  mol h<sup>-1</sup>. The molar Au to benzaldehyde feed rate (*n*/*F*) spanned the range  $1.2 \times 10^{-2}$ – $9 \times 10^{-2}$  h. The reactor effluent was condensed in liquid nitrogen for analysis by capillary GC (Perkin-Elmer Auto System XL). Benzaldehyde (Fluka, ≥98%), benzyl alcohol (Riedel-de Haën, ≥99%) and ethanol (Sigma Aldrich, ≥99%) were used as received. Repeated reaction with different samples from the same batch of catalyst delivered conversion/selectivity values that were reproducible to better than ±5%.

## 3. Results and discussion

### 3.1. Catalyst characterisation

Textural characteristics of the four catalysts considered in this study are given in Table 2. TPR of Au/Al<sub>2</sub>O<sub>3</sub>-DP and Au/Al<sub>2</sub>O<sub>3</sub>-IMP generated profiles shown in Fig. 1 with temperature maxima (*T*<sub>max</sub>) in H<sub>2</sub> consumption at 450 K and 415 K. A single TPR peak over 434–490 K has been reported elsewhere for Au/Al<sub>2</sub>O<sub>3</sub> and ascribed to the reduction of Au<sup>3+</sup> species to Au<sup>0</sup> [18]. The H<sub>2</sub> consumed coincided with that required for precursor reduction (theoretical values recorded in Table 2). The reduction profile for Au/Al<sub>2</sub>O<sub>3</sub>-IMP spanned a lower temperature range than Au/Al<sub>2</sub>O<sub>3</sub>-DP, suggesting weaker precursor–support interactions that result in more facile reduction. Activation

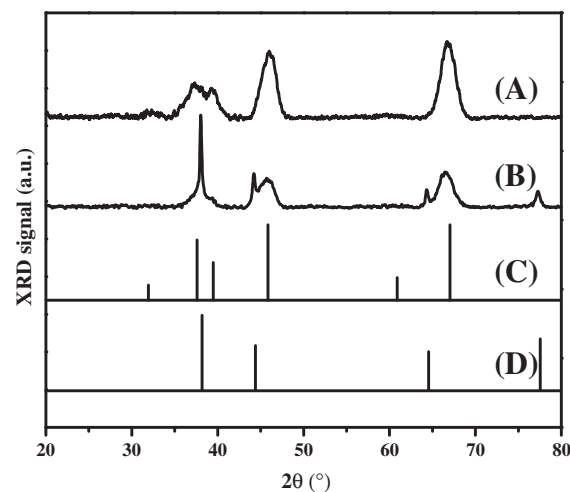


Fig. 2. XRD patterns for (A) Au/Al<sub>2</sub>O<sub>3</sub>-DP and (B) Au/Al<sub>2</sub>O<sub>3</sub>-IMP and JCPDS-ICDD reference for (C) γ-Al<sub>2</sub>O<sub>3</sub> (10-0425) and (D) Au (04-0784).

of Au/ZrO<sub>2</sub> exhibited a similar  $T_{max}$  (452 K) to Au/Al<sub>2</sub>O<sub>3</sub>-DP and matched the requirement for Au<sup>3+</sup> → Au<sup>0</sup> (Table 2). The  $T_{max}$  recorded for Au/TiO<sub>2</sub> reduction was lower than that for Au/Al<sub>2</sub>O<sub>3</sub>-DP. Excess H<sub>2</sub> consumption during the TPR of Au/TiO<sub>2</sub> can be attributed to partial support reduction [19]. Delannoy et al. [20] considered the possible role of the carrier to modify Au precursor reducibility and proposed an order of decreasing reducibility (TiO<sub>2</sub> > CeO<sub>2</sub> > Al<sub>2</sub>O<sub>3</sub>) that is consistent with our results.

Analysis by XRD generated the diffractograms presented in Fig. 2. Au/Al<sub>2</sub>O<sub>3</sub>-DP exhibited diffraction peaks at  $2\theta = 37.6^\circ$ ,  $39.5^\circ$ ,  $45.9^\circ$  and  $67.0^\circ$  corresponding to (311), (222), (400) and (440) planes of  $\gamma$ -Al<sub>2</sub>O<sub>3</sub>. There was no detectable signal due to Au, suggesting a well dispersed Au phase. In contrast, signals at  $38.1^\circ$ ,  $44.3^\circ$ ,  $64.6^\circ$  and  $77.5^\circ$  for Au/Al<sub>2</sub>O<sub>3</sub>-IMP can be assigned to the (111), (200), (220) and (311) planes of Au, diagnostic of larger Au particles. This was confirmed by TEM/STEM analysis and representative images are given in Fig. 3. The Au particles exhibited a quasi-spherical morphology with a narrower distribution of smaller Au particles on Au/Al<sub>2</sub>O<sub>3</sub>-DP (2–8 nm, mean = 4.3 nm) relative to Au/Al<sub>2</sub>O<sub>3</sub>-IMP (1–21 nm, mean = 7.9 nm). This agrees with the literature where catalyst preparation by DP generated smaller Au particles and the residual chloride associated with IMP samples resulted in mobility and agglomeration of Au species during thermal treatment [21]. Gold particle size distribution (2–9 nm, mean = 4.5 nm) on TiO<sub>2</sub> was close to that determined for Au/Al<sub>2</sub>O<sub>3</sub>-DP, whereas Au/ZrO<sub>2</sub> exhibited larger Au size (3–12 nm, mean = 7.0 nm). Hydrogen uptake/activation is a critical catalyst property in hydrogenation applications. We have noted previously [17] that H<sub>2</sub> chemisorption on Au/Al<sub>2</sub>O<sub>3</sub>-IMP at ambient temperature

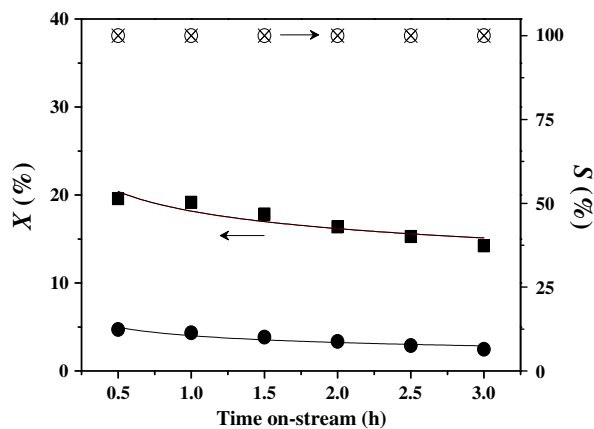


Fig. 4. Temporal variations of conversion (X) and benzyl alcohol selectivity (S) over Au/Al<sub>2</sub>O<sub>3</sub>-DP (■ and ×) and Au/Al<sub>2</sub>O<sub>3</sub>-IMP (● and ○):  $T = 413$  K;  $n/F = 1.2 \times 10^{-2}$  h.

(<1  $\mu\text{mol g}^{-1}$ ) was appreciably lower than that reported for oxide supported transition metals, e.g. Ni/Al<sub>2</sub>O<sub>3</sub> (4  $\mu\text{mol g}^{-1}$ ) and Pd/Al<sub>2</sub>O<sub>3</sub> (24  $\mu\text{mol g}^{-1}$ ). Hydrogen chemisorption on supported Au is an activated process with increased uptake under reaction conditions (45–318  $\mu\text{mol g}_{\text{Au}}^{-1}$  at 413 K, Table 2). Bus et al. [22] have shown that H<sub>2</sub> chemisorption is favoured on smaller Au particles (supported on Al<sub>2</sub>O<sub>3</sub>) that possess a higher fraction of low coordinated Au atoms at corners and edge sites. This agrees with the higher uptake that we have recorded for Au/Al<sub>2</sub>O<sub>3</sub>-DP relative to Au/Al<sub>2</sub>O<sub>3</sub>-IMP.

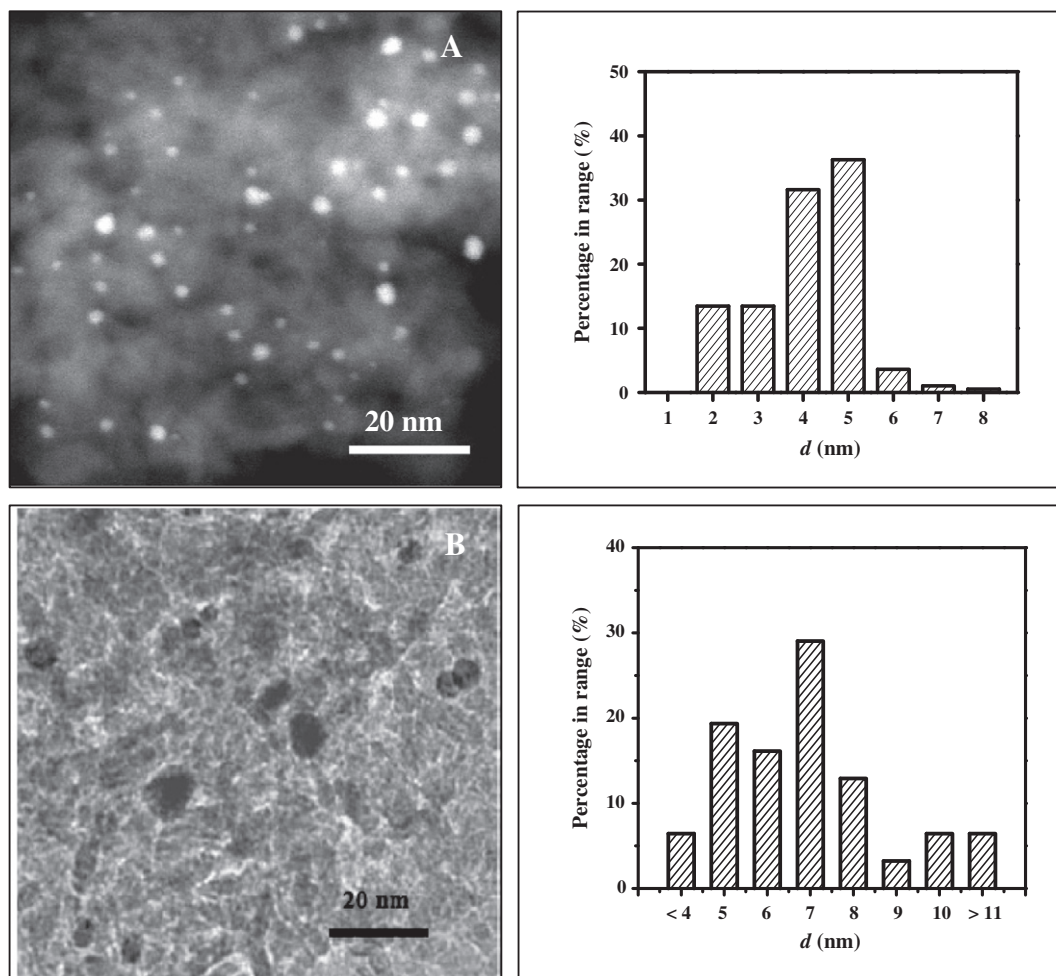


Fig. 3. Representative STEM and TEM images for (A) Au/Al<sub>2</sub>O<sub>3</sub>-DP and (B) Au/Al<sub>2</sub>O<sub>3</sub>-IMP with Au size distribution histograms.

**Table 3**  
Initial conversion ( $X_0$ ) and selectivity ( $S_0$ ) for benzaldehyde hydrogenation over Au/Al<sub>2</sub>O<sub>3</sub>-DP as a function of temperature, contact time and carrier.

T (K)	Carrier	$n/F \times 10^2$ (h)	$X_0$ (%)	$S_0$ (%) benzyl alcohol	$S_0$ (%) toluene
393	Ethanol	1.2	19	100	–
413	Ethanol	1.2	27	100	–
423	Ethanol	1.2	53	92	8
413	Water	1.2	58	100	–
413	Water	9	100	100	–

### 3.2. Catalyst activity and selectivity

Time on-stream conversion ( $X$ ) and benzyl alcohol selectivity ( $S$ ) over Au/Al<sub>2</sub>O<sub>3</sub>-DP and Au/Al<sub>2</sub>O<sub>3</sub>-IMP exhibit a temporal decline (Fig. 4). Initial conversion ( $X_0$ ) can be extracted from fitting the data to

$$\frac{(X-X_0)}{(X_{3\text{ h}}-X_0)} = \frac{\Delta t}{(\beta + \Delta t)}$$

where  $\beta$  is a time scale fitting parameter and  $X_{3\text{ h}}$  is the conversion after 3 h on-stream. Initial conversions were used to determine turnover frequency ( $TOF_0$ , calculated using Au dispersion obtained from TEM analysis) where Au/Al<sub>2</sub>O<sub>3</sub>-DP delivered a significantly higher value ( $86\text{ h}^{-1}$ ) than Au/Al<sub>2</sub>O<sub>3</sub>-IMP ( $30\text{ h}^{-1}$ ). We attribute this to the occurrence of smaller nano-scale Au particles on Au/Al<sub>2</sub>O<sub>3</sub>-DP and greater H<sub>2</sub> uptake (Table 2). Mohr et al. [23] demonstrated structure sensitivity in the hydrogenation of acrolein over Au/ZrO<sub>2</sub> where  $TOF$  increased with decreasing particle diameter (from 8 to 4 nm). However, there is insufficient published data to establish any clear consensus regarding Au size effects in C=O reduction.

The influence of temperature on Au/Al<sub>2</sub>O<sub>3</sub>-DP catalytic response with ethanol as carrier can be assessed from Table 3 where conversion was elevated at higher temperatures with the formation of toluene as by-product (at 423 K). We note that Saadi et al. [13] have reported preferential production of benzyl alcohol over supported Ni and Cu at low reaction temperature (<373 K) with the occurrence of toluene at temperatures >383 K. Exclusivity to the alcohol is challenging as illustrated by the reaction pathways in Fig. 5, where toluene formation occurs via consecutive hydrogenolysis of benzyl alcohol or direct conversion of benzaldehyde. Benzene results from scission of the aldehydic C–H bond [24]; there was no detectable benzene formation in this study. The solvent can influence activity and selectivity, notably in batch liquid operation. Solvent effects in the hydrogenation of unsaturated aldehydes/ketones are associated with polarity, H<sub>2</sub> solubility and surface

**Table 4**  
Initial turnover frequency ( $TOF_0$ ) and selectivity ( $S_0$ ) for benzaldehyde hydrogenation using ethanol and water as carrier:  $T = 413\text{ K}$ ;  $n/F = 1.2 \times 10^{-2}\text{ h}$ .

Catalyst	Carrier	$TOF_0$ (h <sup>-1</sup> )	$S_0$ (%) benzyl alcohol
Au/Al <sub>2</sub> O <sub>3</sub> -DP	Ethanol	86	100
	Water	188	100
Au/TiO <sub>2</sub>	Ethanol	52	100
	Water	98	100
Au/ZrO <sub>2</sub>	Ethanol	37	100
	Water	46	100

interactions [25]. In gas phase applications, the solvent serves as a carrier and possible contributions to catalyst performance have not been studied. Green chemistry principles highlight the use of innocuous (non-toxic) solvents where water can serve as an inexpensive and benign polar solvent. In this study, use of water as carrier resulted in a dramatic increase in conversion, while retaining full selectivity to benzyl alcohol (Table 3). Moreover, an increase in the  $n/F$  parameter, which equates to contact time, resulted in the complete conversion of the inlet benzaldehyde and 100% selectivity to the alcohol. This represents unprecedented selective hydrogenation efficiency with respect to the existing literature (Table 1) for both liquid and gas phase operations.

The beneficial effect of water as carrier in terms of elevated selective hydrogenation rate extended to Au/TiO<sub>2</sub> and Au/ZrO<sub>2</sub> (Table 4). The promotional role of water on C=O reduction in the liquid phase hydrogenation of crotonaldehyde was attributed to facilitated interaction of the hydrophilic C=O moiety with surface catalytic sites [26]. In gas phase hydrogenation over supported Au, activity is limited by available surface reactive hydrogen and any additional hydrogen supply should elevate rate. The generation of surface hydrogen (protons) from water dissociation is promoted by Lewis acid sites on Al<sub>2</sub>O<sub>3</sub> [27] and oxygen vacancies on TiO<sub>2</sub> [28]. The abstracted protons can bond with two-coordinate O<sup>2-</sup> sites on the support to form bridging hydroxyl groups. Buchanan and Web [29] have demonstrated that surface hydroxyl groups on Al<sub>2</sub>O<sub>3</sub> act as a source of atomic ‘hydrogen’ and dehydroxylated Au/Al<sub>2</sub>O<sub>3</sub> was inactive in butadiene hydrogenation. Theoretical calculations have established that the dissociative adsorption of hydrogen on Au (0.16–1.4 eV) [33,34]. Activity of Au/ZrO<sub>2</sub> in the hydrogenation of 1,3-butadiene has been correlated with surface hydroxyl group density where dehydroxylated Au/ZrO<sub>2</sub> was inactive and activity was partially recovered by water treatment [35]. We therefore attribute the beneficial effect of water as carrier to a facilitated surface dissociation that generates reactive hydrogen.

### 4. Conclusion

Gas phase hydrogenation of benzaldehyde over Au supported on Al<sub>2</sub>O<sub>3</sub>, ZrO<sub>2</sub> and TiO<sub>2</sub> was fully selective to benzyl alcohol as the target product. Increased benzaldehyde  $TOF$  over Au/Al<sub>2</sub>O<sub>3</sub> prepared by deposition–precipitation is associated with increased H<sub>2</sub> uptake on well dispersed Au (mean particle size = 4.3 nm) relative to synthesis by impregnation (mean = 7.9 nm). Use of an aqueous rather than ethanolic benzaldehyde feed delivered appreciably higher chemoselective rates with 100% benzyl alcohol yield. This is attributed to water dissociation on the catalyst surface, generating reactive hydrogen that compensates for the limited capability of Au to dissociate H<sub>2</sub>, with an overall increased hydrogenation rate. This promotional effect extends to benzaldehyde conversion over Au/ZrO<sub>2</sub> and Au/TiO<sub>2</sub>.

### Acknowledgements

We acknowledge Dr. F. Cárdenas-Lizana and Yufen Hao for contributions to this work and financial support to M.L. and X.W. through the Overseas Research Students Award Scheme.

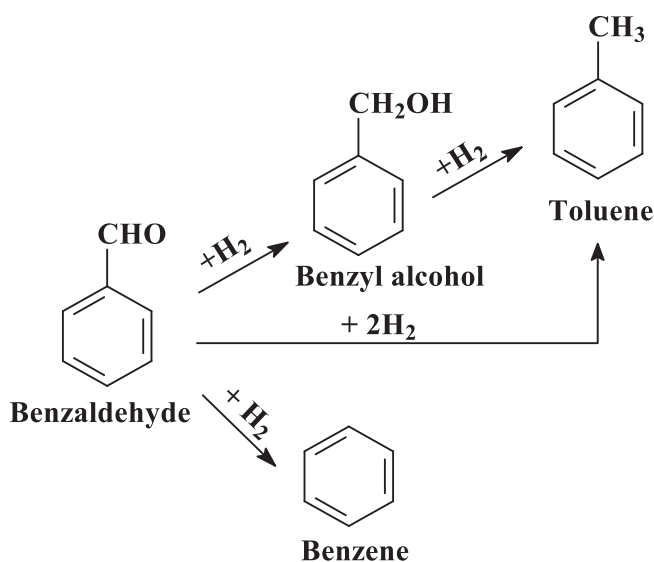


**Fig. 5.** Reaction pathways in the hydrogenation of benzaldehyde.

## References

- [1] J. Scognamiglio, L. Jones, D. Vitale, C.S. Letizia, A.M. Api, *Food Chem. Toxicol.* 50 (2012) S140–S160.
- [2] G.D. Yadav, P.H. Mehta, *Catal. Lett.* 21 (1993) 391–403.
- [3] C.C. Guo, Q. Liu, X.T. Wang, H.Y. Hu, *Appl. Catal. A Gen.* 282 (2005) 55–59.
- [4] B.R. Cho, R.M. Laine, *J. Mol. Catal.* 15 (1982) 383–389.
- [5] D. Tavor, O. Sheviev, C. Dlugy, A. Wolfson, *Can. J. Chem.* 88 (2010) 305–308.
- [6] X.D. Xu, H. Vonk, A. van de Riet, A. Cybulski, A. Stankiewicz, J.A. Moulijn, *Catal. Today* 30 (1996) 91–97.
- [7] M. Arai, A. Obata, Y. Nishiyama, *J. Catal.* 166 (1997) 115–117.
- [8] M. Baidossi, A.V. Joshi, S. Mukhopadhyay, Y. Sasson, *Synth. Commun.* 34 (2004) 643–650.
- [9] M. Okamoto, T. Hirao, T. Yamaai, *J. Catal.* 276 (2010) 423–428.
- [10] F.Y. Zhao, S. Fujita, S. Akihara, M. Arai, *J. Phys. Chem. A* 109 (2005) 4419–4424.
- [11] D. Haffad, U. Kameswari, M.M. Bettahar, A. Chambellan, J.C. Lavalley, *J. Catal.* 172 (1997) 85–92.
- [12] M.A. Vannice, D. Poondi, *J. Catal.* 169 (1997) 166–175.
- [13] A. Saadi, Z. Rassoul, M.M. Bettahar, *J. Mol. Catal. A Chem.* 164 (2000) 205–216.
- [14] A. Saadi, R. Merabiti, Z. Rassoul, M.M. Bettahar, *J. Mol. Catal. A Chem.* 253 (2006) 79–85.
- [15] P. Claus, *Appl. Catal. A Gen.* 291 (2005) 222–229.
- [16] L. McEwan, M. Julius, S. Roberts, J.C.Q. Fletcher, *Gold Bull.* 43 (2010) 298–306.
- [17] N. Perret, F. Cardenas-Lizana, M.A. Keane, *Catal. Commun.* 16 (2011) 159–164.
- [18] F. Cardenas-Lizana, S. Gomez-Quero, M.A. Keane, *Catal. Lett.* 127 (2009) 25–32.
- [19] X.D. Jiang, Y.P. Zhang, J. Jiang, Y.S. Rong, Y.C. Wang, Y.C. Wu, C.X. Pan, *J. Phys. Chem. C* 116 (2012) 22619–22624.
- [20] L. Delannoy, N. Weiher, N. Tsapatsaris, A.M. Beesley, L. Nchari, S.L.M. Schroeder, C. Louis, *Top. Catal.* 44 (2007) 263–273.
- [21] G.C. Bond, D.T. Thompson, *Catal. Rev. Sci. Eng.* 41 (1999) 319–388.
- [22] E. Bus, J.T. Miller, J.A. van Bokhoven, *J. Phys. Chem. B* 109 (2005) 14581–14587.
- [23] C. Mohr, H. Hofmeister, P. Claus, *J. Catal.* 213 (2003) 86–94.
- [24] M.A. Keane, *J. Mol. Catal. A Chem.* 118 (1997) 261–269.
- [25] U.K. Singh, M.A. Vannice, *Appl. Catal. A Gen.* 213 (2001) 1–24.
- [26] M.-M. Wang, L. He, Y.-M. Liu, Y. Cao, H.-Y. He, K.-N. Fan, *Green Chem.* 13 (2011) 602–607.
- [27] K.C. Hass, W.F. Schneider, A. Curioni, W. Andreoni, *Science* 282 (1998) 265–268.
- [28] J. Oviedo, R. Sanchez de Armas, M.A. San Miguel, J.F. Sanz, *J. Phys. Chem. C* 112 (2008) 17737–17740.
- [29] D.A. Buchanan, G. Webb, *J. Chem. Soc. Faraday Trans.* 71 (1975) 134–144.
- [30] Y.L. Liu, Y.W. Hua, M. Jiang, G. Jiang, J. Chen, *J. Chem. Phys.* 136 (2012) 084703.
- [31] J.L.C. Fajin, M. Cordeiro, J.R.B. Gomes, *J. Mol. Struct. (Theochem)* 946 (2010) 51–56.
- [32] G.-C. Wang, S.-X. Tao, X.-H. Bu, *J. Catal.* 244 (2006) 10–16.
- [33] A. Zanchet, A. Dorta-Urra, O. Roncero, F. Flores, C. Tablero, M. Paniagua, A. Aguado, *Phys. Chem. Chem. Phys.* 11 (2009) 10122–10131.
- [34] Z. Li, Y.X. Li, J.L. Li, *J. Chem. Phys.* 137 (2012) 234704.
- [35] X. Zhang, H. Shi, B.-Q. Xu, *J. Catal.* 279 (2011) 75–87.